Preparation and characterization of a novel sulfonated titanium oxide incorporated Chitosan nanocomposite membranes for fuel cell application

Saad Ahmed
University of Okara
Amjad Hussain
University of Okara
Tasleem Arshad
University of Okara
Muhammad Khan
University of Okara
Amir Zada (amistry009@yahoo.com)
Abdul Wali Khan University Mardan https://orcid.org/0000-0003-3670-4408
Muhammad Hassan
East China University of Science and Technology School of Chemistry and Molecular Engineering
Hidayat Hussain
Leibniz Institute of Plant Biochemistry: Leibniz-Institut fur Pflanzenbiochemie
Javid Hussain
University of Nizwa
Muhammad Imran
King Khalid University
Iftikhar Ali
Karakoram University: Karakoram International University
Ikram Ahmad
University of Sahiwal
Maroof Ali
Anhui Normal University
Hussain Ullah
University of Okara

Research Article

Keywords: Sulfonated TiO2, chitosan, sulfonic group, stability, proton exchange membrane fuel cell

Posted Date: March 11th, 2021

DOI: https://doi.org/10.21203/rs.3.rs-276858/v1

Version of Record: A version of this preprint was published on June 17th, 2021. See the published version at https://doi.org/10.3390/membranes11060450.

Abstract

In this study, nano-TiO_2 sulfonated ($STiO_2$) with 1,3-propanesultone was incorporated into the chitosan matrix for the fabrication of chitosan/$STiO_2$ ($C/STiO_2$) nanocomposite membranes. The grafting of sulfonic acid ($–SO_3H$) groups was confirmed with Fourier transform infrared spectroscopy, thermos-gravimetric analysis and energy-dispersive X-ray spectroscopy. The physicochemical properties such as water uptake, swelling ratio, thermal and mechanical stability, ion exchange capacity and proton conductivity of the as prepared membranes were measured. The proton groups on the surface of TiO_2 can form continuous proton conducting pathways along the $C/STiO_2$ interface resulting in the improvement of proton conductivity of $C/STiO_2$ nanocomposite membranes. The nanocomposite membrane with 5 % sulfonated TiO_2 showed higher proton conductivity (0.035 S·cm-1) than commercial Nafion-117 membrane (0.033 S·cm-1) due to the strong interfacial interactions between -SO_3H group of acid and hydroxyl group of TiO_2. Further, the $–NH_2$ groups of chitosan restrict the mobility of chitosan chains to enhance the thermal and mechanical stability of the nanocomposite membranes. These $C/STiO_2$ nanocomposite membranes have promising applications in proton exchange membrane fuel cells.

1. Introduction

The increasing environmental pollution and depleting natural resources have emphasized the need for clean and sustainable energy [1–7]. One of the most effective methods for this purpose is the conversion of chemical energy into electrical energy [8–9]. In recent years, proton exchange membrane fuel cells (PEMFCs) have fascinated much consideration in energy fields owing to their high effectiveness and environmental friendliness [10–13]. Perfluorosulfonic polymer-based membranes such as Nafion have high proton conductivity and notable mechanical and chemical stability due to the particular structure of Nafion [14–17]. However, the practical applicability of Nafion is restricted by its high price and sudden decline in proton conductivity at temperatures higher than 100°C. Chitosan has the advantages of low cost, ophilicity and environmental benefits, making it attractive for various applications such as food packaging, drug delivery and PEMs [18–22]. However, its proton conductivity is much lower than that of Nafion, which represents a major hindrance to the applications of chitosan-based membranes.

Organic/inorganic composites are composed of the polymer matrix and inorganic fillers [23]. They have been widely utilized in different fields such as ultrafiltration, pervaporation, dye-sensitized solar cells, lithium-ion batteries and biosensors [24–28]. Various inorganic fillers, such as TiO_2, zirconium oxide, halloysite, and graphene oxide have been introduced into the polymer matrix for the fabrication of PEMs to improve their mechanical and thermal stabilities as well as the proton conductivity [29–34]. Incorporating acid-grafted inorganic fillers into the polymer matrix can also increase the proton conductivity and the interfacial compatibility of the composite membranes [35–41].

TiO_2 as semiconductor photocatalysts has been widely applied in photocatalysis for water splitting, CO_2 reduction, pollutants degradation and bacterial disinfection. It has been used in solar cells due to its hydrophilic and ultraviolet resistance nature [42–50]. Therefore, the introduction of TiO_2 as inorganic filler will certainly improve the thermal and chemical stabilities of the fabricated membranes for the increased proton conductivity in fuel cells.

In this study, a novel sulfonated TiO_2 was prepared and embedded into the chitosan matrix to prepare C/$STiO_2$ nanocomposite membranes. These sulfonated TiO_2 particles and C/$STiO_2$ nanocomposite membranes were characterized by Fourier transform infrared (FTIR) spectroscopy, energy-dispersive X-ray (EDX) spectroscopy, X-ray diffraction (XRD) analysis, scanning electron microscopy (SEM), and thermogravimetric analysis (TGA). The effects of sulfonated TiO_2 particles ($STiO_2$) on the physicochemical properties of C/$STiO_2$ membranes, including water uptake, area swelling, ion exchange capacity (IEC), and proton conductivity were investigated. The interfacial interactions among the -SO_3H groups of $STiO_2$ and the -NH_2 groups of chitosan could offer uninterrupted proton conducting pathways, making it possible to enhance the proton conductivity along with mechanical stability of membranes.

2. Experimental

2.1 Materials and chemicals

Chitosan with a de-acetylation value of ≥ 80% and rutile-type titanium dioxide powder with particle size of 80 nm were purchased from Aladdin Chemical Reagent Co. (China). Acetic acid (99%), sulfuric acid (98%) and 1, 3-propanesultone were purchased from Macklin Biochemical Co., Ltd., (China). Absolute ethyl alcohol ≥ 99.8% and deionized water were used during the experiments.

2.2. Sulfonation of Nano-TiO_2

For the sulfonation of nano-TiO_2, 1 g TiO_2 was dispersed in 22 ml of a solution of 1, 3-propanesultone in toluene (volumetric ratio of 1: 11). The mixture was refluxed at 110°C for 24 h and the obtained sulfonated titania ($STiO_2$) was centrifuged, washed several times with water and absolute ethyl alcohol, and finally dried at 80°C for 24 h. This experimental procedure is given in Fig. 1.

2.3. Incorporation of $STiO_2$ in chitosan matrix

C/$STiO_2$ nanocomposite membranes with different $STiO_2$ contents were fabricated as follows: 1.5 g of chitosan were dissolved in 2% W/W aqueous solution of acetic acid under constant stirring. A certain amount of $STiO_2$ was ultrasonically dispersed in 2% W/W aqueous solution of acetic acid at 300 W and 40 Hz for 1 h. The two mixtures were homogenously mixed at 80°C and degassed for 1 h. After cooling to room temperature, the sample was transferred to a clean glass plate and dried in an oven at 40°C for 24 h. The obtained membrane was cross-linked with 1 M H_2SO_4 solution for 48 h and the product was washed with deionized water to remove the extra acid and dried under vacuum at 25°C for 24 h. In this way, different C/$STiO_2$ membranes with 1, 3, 5 and 7% of $STiO_2$ were prepared and named as C/1$STiO_2$,

C/3STiO$_2$, C/5STiO$_2$ and C/7STiO$_2$ respectively. For compassion, pure chitosan membrane was prepared by the same method without adding STiO$_2$.

2.4. Characterization

The FTIR spectra of STiO$_2$ and C/STiO$_2$ nanocomposite membranes were recorded in transmittance mode in the range of 500–4000 cm^{-1} at a scan rate of 4 cm^{-1} at room temperature using a Nicolet 6700 FTIR spectrometer. The phase identification and crystalline structure of C/STiO$_2$ nanocomposite membranes were determined with Rigaku D/max diffractometer (2550 VB/PC: CuKα; λ = 0.154 nm radiation) at an operating current and voltage of 40 mA and 40 kV respectively. The cross-sectional morphologies of the membranes were characterized with SEM (FE-S4800, Hitachi) equipped with an EDX spectroscope at an accelerating voltage of 200 kV. TGA was performed using a TA 50 thermogravimetric analyzer under nitrogen atmosphere at a rate of 10°C min^{-1} from 25°C to 700°C. The mechanical properties were determined using a MTS E43 universal testing machine according to Chinese standard GB.T.1040.3 at an initial speed of 2 mm/min at room temperature

2.5. Measurement of water and methanol uptake and swelling ratio

The water uptake of C/STiO$_2$ membranes was measured by the weight difference between dry membranes (W_{dry}) and membranes dipped in water (W_{wet}) for 24 h at room temperature. The methanol uptake was measured in a similar manner except that the membranes were dipped in 2M methanol aqueous solution as given in equation 1. In order to measure the swelling ratio, a piece of dry C/STiO$_2$ nanocomposite with an area of 2.0 cm × 1.0 cm (A_{dry}) was immersed in water for 24 h at room temperature and its area in cm^2 was re-measured (A_{wet}), as shown in equation 2.

$$\text{Uptake (\%)} = \frac{W_{wet} - W_{dry}}{W_{dry}} \times 100 \qquad \text{Eq (1)}$$

$$\text{Area swelling (\%)} = \frac{A_{wet} - A_{dry}}{A_{dry}} \times 100 \qquad \text{Eq (2)}$$

2.6. Calculation of ion exchange capacity (IEC)

The IECs of C/STiO$_2$ membranes were calculated by classical acid-base titration method. A pre-weighted membrane was dipped in a saturated NaCl solution for 48 h to achieve complete exchange of H^+ with Na^+. The solution was then titrated with 0.01 M NaOH solution using phenolphthalein as indicator at room temperature. The IEC value was calculated from Eq. 3 as:

$$\text{IEC (mmolg}^{-1}) = \frac{0.01 \times 1000 \times V_{NaOH}}{W_{dry}} \qquad \text{Eq (3)}$$

Where V_{NaOH} is the used volume (mL) of NaOH solution and W_{dry} is the weight of the dry membrane.

2.7. Measurement of proton conductivity

The proton conductivity of C/$STiO_2$ nanocomposites was measured by AC impedance spectroscopy with an electrochemical workstation (PARSTAT 2273 AMETEK, Inc., America) at a frequency of 1– 10^6 Hz and an oscillating voltage of 20 mV. Before analysis, all samples were dipped in 0.2 M H_2SO_4 for 24 h. The hydrated membranes (2 cm×0.5 cm) were fit in among the two electrodes of the polytetrafluoroethylene (PTFE) mould at room temperature with 100% RH and the proton conductivity was calculated as:

$$\sigma = \frac{L}{RA} \qquad \text{Eq (4)}$$

Where L (cm), A (cm^2) and R (Ω) are the thickness, area and resistance of the membrane respectively.

3. Results And Discussion

3.1. Characterization of $STiO_2$

The surface modification of TiO_2 was characterized by FTIR, TGA and EDX. The characteristic bands at 1631 and 3417 cm^{-1} in Fig. 2(a) are due to the –OH bending and stretching vibration, respectively. $STiO_2$ shows two new bands at 1045 cm^{-1} and 1213 cm^{-1} suggesting the successful grafting of sulfonic acid groups on TiO_2 with a significant reduction in hydroxyl groups [51].

The TGA curve displays a three-stage weight loss process (Fig. 2(b) and Table 1). The first stage is attributed to the evaporation of physically adsorbed water while the second stage is due to the loss of organic matter. However, there is a negligible weight loss at above 400 ºC. Upon further heating, the weight loss is related to the decomposition of grafted chains. Moreover, $STiO_2$ shows a higher weight loss than TiO_2, suggesting that $STiO_2$ has abundant sulfonic acid groups.

Table 1
TGA analysis of TiO_2 and $STiO_2$

Serial No.	T5%	Char residue (wt. %)			
		500°C	600°C	700°C	800°C
TiO_2	420.30	92.39	91.68	91.31	90.93
$STiO_2$	256.24	89.08	88.60	88.47	88.24

The EDX results (Table 2) show that pristine TiO_2 has no sulfur whereas $STiO_2$ contains sulfur resulting from the reaction with 1,3-propanesultone, suggesting that sulfonic acid groups have been grafted onto TiO_2 surface.

Table 2
Atomic composition (%) of Ti, O and S in pristine TiO_2 and $STiO_2$

Serial No.	Ti	O	S
TiO_2	22.71	77.29	–
$STiO_2$	23.43	74.57	2.00

3.2. Structural characterization of C/$STiO_2$ membranes

Figure 3 shows the FTIR spectra of C/$STiO_2$ membranes with different $STiO_2$ contents. The characteristic peaks at 1650 and 1558 cm^{-1} are attributed to the bending vibration of $-NH_2$. The broad peak at 3426 cm^{-1} is attributed to -OH stretching [6]. The characteristic peaks at 2932 cm^{-1} and 1375 cm^{-1} are attributed to -CH stretching and $-CH_3$ symmetric deformation, respectively [52]. After cross-linking with H_2SO_4, the characteristic peaks at 1656 and 1598 cm^{-1} shift to lower wave number side, suggesting that the $-NH_2$ of chitosan is protonated. This is endorsed to shift of hydrogen bond structure and change in intensity in chitosan molecules [53]. Enhancing the $STiO_2$ content in nanocomposites, the bands at 3600 – 3000 cm^{-1} and 1656 – 1592 cm^{-1} are shifted to lower wave number side in C/$STiO_2$ membranes. This phenomenon corresponds to the formation of strong interfacial attractions among $-SO_3H$ of $STiO_2$ and –OH/$-NH_2$ of chitosan molecules.

Chitosan molecules have a high degree of crystallinity owing to the strong intermolecular and intramolecular interactions. As the proton mobility and diffusion of water molecules in PEMs often take place in an amorphous phase, it is necessary to convert crystalline phase chitosan into semi-crystalline or amorphous phase. The impact of $STiO_2$ on the crystalline nature of chitosan was determined by XRD. The characteristic peak at 12° depicts the hydrated crystalline section in chitosan molecules, whereas that at 23° depicts the amorphous section. However, the incorporation of $STiO_2$ results in a decrease peak intensity at 19 and 23° (Fig. 4). The decrease in the crystalline region is endorsed to the presence of hydrogen and electrostatic interaction between chitosan molecules and $STiO_2$ that can interfere with order packing of chitosan chain and subsequently diminish its crystalline region. The other peaks at 27, 36, 44 and 56° confirm the presence of rutile phase titania [54].

C/$STiO_2$ membranes were fabricated by solution casting method using chitosan as the polymer matrix and $STiO_2$ as the nanofillers. Figure 5 shows the cross sectional morphologies of pure chitosan and

C/$STiO_2$ membranes. Pure chitosan shows a cross-sectional structure with no obvious defects or cracks. However, as the $STiO_2$ content increases, a stacked structure is observed in C/$STiO_2$ membranes, and $STiO_2$ particles are homogeneously dispersed in the chitosan matrix with no agglomeration, which can be due to strong electrostatic interactions between the polymer and nanofillers. This results in the formation of uninterrupted proton transfer pathways and consequently an improvement of the proton conductivity of C/$STiO_2$ resultant membranes.

3.3. Thermal and mechanical stability of C/$STiO_2$ nanocomposite membranes

The thermal stability of C/$STiO_2$ membranes was determined from their TGA thermograms (Fig. 6). Pure chitosan membrane shows a three-stage weight loss process. The initial stage at 30–200°C is assigned to the evaporation of adsorbed water, the second one at 215–330°C is due to the degradation of chitosan side chains and the last one at 480–800°C corresponds to the degradation of polymer backbone [55]. However, the incorporation of $STiO_2$ retards the degradation of chitosan molecules and thus improves the thermal strength of C/$STiO_2$ membranes. This is mainly due to the interfacial interactions (hydrogen bonding or electrostatic interactions) that can interfere with the order packing of chitosan chains and thus hinder the degradation of polymer backbone of chitosan molecule. The remaining weight of chitosan at 750°C is 21.03%, and as the $STiO_2$ content increases from C/1$STiO_2$ to C/7$STiO_2$, the residual weight increases from 27.37 to 29.73%.

It is crucial for PEMs to have sufficiently high mechanical stability, which can have major impacts on the durability of PEMFCs. Table 3 shows that all C/$STiO_2$ membranes have higher tensile strength than pristine nanocomposite membrane (13.05 MPa). As the $STiO_2$ content increases from C/1$STiO_2$ to C/7$STiO_2$, the tensile strength increases from 17.84 to 25.30 MPa, which is endorsed to (a) the increase of columbic interactions among the amine groups of chitosan and the $–SO_3H$ groups of TiO_2 and (b) the hydrogen bonding between $–SO_3H$ of $STiO_2$ and –OH or $–NH_2$ groups of chitosan. These electrostatic interactions can restrict the mobility of chitosan chains and subsequently increase the tensile strength of C/$STiO_2$ membranes. The $–SO_3H$ has a polar and ionic nature, and a proper concentration of sulfonic acid groups can result in the formation of ionic clusters in the chitosan matrix, which consequently increases the tensile strength of C/$STiO_2$ nanocomposite membranes. C/7$STiO_2$ nanocomposite membrane shows higher tensile strength than Nafion 117 membrane (23.6 MPa). The elongation at break (%) of the nanocomposite membranes is also improved compared with that of pure chitosan membrane. $STiO_2$ can halt the propagation of micro-cracks owing to the strong interfacial interactions between $STiO_2$ and the chitosan matrix, thus resulting in an enhancement of the elongation at break of all nanocomposite membranes.

Table 3
Mechanical properties of chitosan control and C/$STiO_2$ nanocomposite membranes

Membranes	Tensile strength (MPa)	Elongation at break (%)
Chitosan	13.05 ± 1.03	15.61 ± 6.98
C/1$STiO_2$	17.84 ± 2.02	23.54 ± 2.22
C/3$STiO_2$	21.32 ± 3.33	19.57 ± 4.20
C/5$STiO_2$	23.27 ± 0.92	21.59 ± 5.70
C/7$STiO_2$	25.30 ± 2.69	19.34 ± 4.35

3.4. Water and methanol uptake, dimensional stability and IEC of C/$STiO_2$ membranes

The hydrolytic stability of C/$STiO_2$ membranes was measured to evaluate their applicability in PEMFCs. Water uptake is expected to have significant impacts on the mechanical characteristics and proton conductivity of polymer electrolyte membranes. The existence of water within the membrane can assist the dissociation of various functional groups that is essential to achieve high proton conductivity. However, unnecessary water uptake can lead to dimensional instability in fuel cell assembly. The water uptake of pristine chitosan membrane is as high as 65% owing to the presence of hydrophilic -OH and -NH_2 of chitosan (Fig. 7a). However, increase in the $STiO_2$ content results in a decrease of the water uptake from 58 to 51%. The addition of $STiO_2$ rigidifies chitosan molecules, thus making it less capable of adsorbing solvent molecules [30]. The columbic and hydrogen bonding interactions between the –SO_3H groups of $STiO_2$ and the –NH_2 and -OH groups of chitosan also reduce the water adsorption capacity of C/$STiO_2$ nanocomposite membranes. The incorporation of $STiO_2$ can hinder the mobility of chitosan chains and reduce water storing sites, which results in reduction of water uptake of C/$STiO_2$ nanocomposite membranes [56, 57].

The methanol uptake is also important for nanocomposite membranes for use in PEMFCs. It is desirable for PEMs to have lower methanol absorption as high methanol uptake can lead to fuel crossover and thus reduce cell efficiency. Pure chitosan membrane shows a methanol uptake of 56%. As the $STiO_2$ content increases from C/1$STiO_2$ to C/7$STiO_2$, the methanol uptake decreases from 46 to 42% (Fig. 7b). The methanol uptake of PEMs depends greatly on the available space within the membranes. Water is more polar than methanol, making it easier to access the hydrophilic domains in a membrane. As the $STiO_2$ content increases, the diffusion capacity of nanocomposite membranes for methanol is suppressed. Hence, the methanol uptake of the nanocomposite membranes decreases.

The swelling via hydration can cause dimensional instability of PEMs. The area swelling of chitosan control and C/$STiO_2$ nanocomposite membranes are shown in Fig. 7c. It is noted that the incorporation of

$STiO_2$ results in decrease in both water uptake and area swelling of the nanocomposite membranes. The swelling of these $C/STiO_2$ membranes can also be reduced as $STiO_2$ can inhibit the swelling of chitosan matrix. The chitosan membrane shows an area swelling of 60%, whereas that of $C/7STiO_2$ membrane is significantly reduced to 42%.

The number of ionizable hydrophilic functional groups in the membrane gives a reliable estimation of the proton conductivity. Figure 7d shows that the chitosan membrane has an IEC value of 0.125 mmol g^{-1}. In comparison, increasing the $STiO_2$ content from $C/1STiO_2$ to $C/7STiO_2$ results in an increase of IEC value from 0.153 to 0.220 mmol g^{-1}, which is mainly endorsed to the presence of proton conducting (SO_3H) groups in the chitosan matrix.

3.5. Electrochemical characteristics of $C/STiO_2$ membranes

The proton conductivity is primarily determined by water content, distribution of water molecules and the formation of ionic clusters within a PEM. Theoretically, there are two mechanisms for proton transfer in a membrane, including the Vehicle mechanism whereby protons are transported in the form of hydrated hydrogen ions, and the Grotthuss mechanism whereby protons are transported from one carrier to the next through hydrogen bonding network [58, 59]. The chitosan membrane displays a proton conductivity of 0.011 $S{\cdot}cm^{-1}$, which is reliable with earlier report. The proton conductivity of Nafion 117 (0.033 $S{\cdot}cm^{-1}$) is used for assessment in this study. The increase of the $STiO_2$ content from 1 to 7% results in enhancement of the proton conductivity from 0.019 to 0.035 $S{\cdot}cm^{-1}$ as presented in Fig. 8. There are abundant sulfonic acid groups in the polymer matrix that can offer extra proton hopping sites. The homogeneous dispersion of $STiO_2$ can offer uninterrupted proton transfer pathways through which protons can migrate rapidly. Increasing the $STiO_2$ content can increase the number of ion-exchangeable sites per cluster that can improve the proton mobility within a membrane. Furthermore, the generation of acid-base pairs at the $C/STiO_2$ interface can also facilitate the protonation/deprotonation process. All of these could contribute to improve the proton conductivity of the nanocomposite membranes. $C/5STiO_2$ nanocomposite membrane shows a higher proton conductivity (0.035 $S{\cdot}cm^{-1}$) than commercially available Nafion 117 membranes (0.033 $S{\cdot}cm^{-1}$).

Conclusions

In this study, a novel one step approach was proposed for the preparation of $STiO_2$. The $C/STiO_2$ nanocomposite membranes were fabricated by solution casting method for PEMFC applications. These membranes show lower water and methanol uptake and better dimensional stability than chitosan membranes. Their thermal and mechanical stability can be improved due to inhibited mobility of chitosan chains. $C/5STiO_2$ membrane shows higher proton conductivity than Nafion 117 membrane. These outcomes may probe a simple strategy for fabrication of chitosan based PEMs, which has a promising potential in the application of electrochemical devices.

Declarations

Acknowledgments

This research is financially supported by the National Natural Science Foundation of China (51463020), Kunlun Scholar Award Program of Qinghai Province and Thousand Talents Program of Qinghai Province.

References

[1] Y. Qu, Tsen W.C., Jang S.C., Chuang F.S., Wang J., Liu H., Wen S., Gong C. Novel composite polymer electrolyte membrane using solid superacidic sulfated zirconia-functionalized carbon nanotube modified chitosan, Electrochim. Acta. 264 (2018) 251-259. doi: 10.1016/j.electacta.2018.01.131.

[2] O. Ying, T. Wen-Chin, G. J. Wang, H. Liu, G. Zheng, C. Qin, S. Wen, Chitosan-based composite membranes containing chitosan-coated carbon nanotubes for polymer electrolyte membranes, Polym. Adv. Technol. 2018, 29:612-622. doi: 10.1002/pat.4171.

[3] V. Vijayalekshmi, D. Khastgir, Chitosan/partially sulfonated poly(vinylidene fluoride) blends as polymer electrolyte membranes for direct methanol fuel cell applications, Cellulose 25 (2018) 661-681, https://doi.org/10.1007/s10570-017-1565-6.

[4] M. Khan, N. Shahzad, C. Xiong, T. K. Zhao, T. Li, F. Siddique, N. Ali, M. Shahzad, H. Ullah, S. A. Rakha, Dispersion behavior and the influences of ball milling technique on functionalization of detonated nano-diamonds, Diamond Relat. Mater. 61 (2016) 32-40.

[5] M. Tariq, W. Q. Zaman, W. Sun, Z. Zhou, Y. Wu, L. Cao, J. Yang, Unraveling the beneficial electrochemistry of IrO_2/MoO_3 hybrid as a highly stable and efficient oxygen evolution reaction catalyst, ACS Sust. Chem. Eng. 6 (2018) 4854-4862. https://doi.org/10.1021/acssuschemeng.7b04266

[6] S. Ahmed, Y. Cai, M. Ali, S. Khanal, S. Xu, Chitosan/titanate nanotube hybrid membrane with low methanol crossover for direct methanol fuel cells, J. Appl. Polym. Sc. (2018) 46904, doi.org/10.1002/ceat.200900443

[7] A. Antelava, A. Constantinou, A. Bumajdad, G. Manos, R. Dewil, S. M. Al-Salem (2020) Identification of commercial oxo-biodegradable plastics: study of UV induced degradation in an effort to combat plastic waste accumulation. J Polym Environ 28:2364.

[8] N. Shaari, S.K. Kamarudin, Chitosan and alginate types of bio-membrane in fuel cell application: An Overview, J. Power Sources, 289 (2015): 71. doi: 10.1016/j.jpowsour.2015.04.027.

[9] M. Khan, A. A. Khurram, L. Tiehu, T. K. Zhao, C. Xiong, Z. Ali, N. Ali, A. Ullah, Reinforcement effect of acid modified nanodiamond in epoxy matrix for enhanced mechanical and electromagnetic properties, Diamond Relat. Mater. 78 (2017) 58-66; doi.org/10.1016/j.enconman.2009.11.017

[10] S. Ahmed. M. Ali, Y. Cai, Y. Lu, Z. Ahmad, S. Khannal, S. Xu, Novel sulfonated multi-walled carbon nanotubes filled chitosan composite membrane for fuel-cell applications, J. Appl. Polym. Sci. 136 (2019) 47603. doi.org/10.1002/app.47603

[11] Q. Tang, J. Wu, Z. Tang, Y. Lia, J. Lin, High-temperature proton exchange membranes from ionic semiconductive materials, J. Mater. Chem. 22 (2012) 15836; doi:10.1039/C2JM32637J

[12] M.J. Parnian, S. Rowshanzamir, F. Gashoul, Comprehensive investigation of physicochemical and electrochemical properties of sulfonated poly (ether ether ketone) membranes with different degrees of sulfonation for proton exchange membrane fuel cell applications, Energy 125 (2017) 614-628. doi.org/10.1016/j.energy.2017.02.143

[13] S. Ahmed, Y. Cai, M. Ali, S. Khannal, S. Xu, Preparation and properties of alkyl benzene sulfonic acid coated boehmite/chitosan nanocomposite membranes with enhanced proton conductivity for proton exchange membrane fuel cells, Mater. Express, 9 (2019) 42.

[14] F. K. Molavi, I. Ghasemi, M. Messori, M. Esfandeh (2019) Design and characterization of novel potentially biodegradable triple-shape memory polymers based on immiscible poly(L-lactide)/poly(□-caprolactone) blends. J Polym Environ 27:632

[15] S.P. Nunes, B. Ruffmann, E. Rikowski, S. Vetter, K. Richau, Inorganic modification of proton conductive polymer membranes for direct methanol fuel cells, J. Membr. Sci. 203 (2002) 215; doi.org/10.1016/S0376-7388(02)00009-1

[16] B. Liu, P. Gilles, D. Kim, M. D. Guiver, W. Hu, Z. Jiang, Aromatic poly(ether ketone)s with pendant sulfonic acid phenyl groups prepared by a mild sulfonation method for proton exchange membranes, Macromol. 40 (2007) 1934-1944.

[17] P. Khomein, W. Ketelaars, T. Lap, G. Liu, Sulfonated aromatic polymer as a future proton exchange membrane: A review of sulfonation and crosslinking methods, Renew. Sust. Energy Rev. 137 (2021) 110471; https://doi.org/10.1016/j.rser.2020.110471

[18] N. Ciftci, I. Sargin, G. Arslan, U. Arslan, A. Okudan. (2020) Ascorbic acid adsorption-release performance and antibacterial activity of chitosan-ter(GMA-MA-NTBA) polymer microcapsules. J Polym Environ 28: 2277

[19] E. Atangana, P. J. Oberholster. (2020) Modified biopolymer (chitin-chitosan derivatives) for the removal of heavy metals in poultry wastewater. J Polym Environ 28:388.

[20] D. Liu, Y. Xie, N. Cui, X. Han, J. Zhang, J. Pang, Z. Jiang, Structure and properties of sulfonated poly(arylene ether)s with densely sulfonated segments containing mono-, di- and tri-tetraphenylmethane as proton exchange membrane, J. Membr. Sci. (2020) 118856, doi.org/10.1016/j.memsci.2020.118856

[21] Y. Y. Cai, Q. Yang, L. X. Sun, Z. Y. Zhu, Q. G. Zhang, A. M. Zhu, Q. L. Liu, Bioinspired layered proton-exchange membranes with high strength and proton conductivity, Int. J. Hydrogen Energy (2020) doi.org/10.1016/j.ijhydene.2020.10.198

[22] N. Ali, Awais, T. Kamal, M. U. Islam, A. Khan, S. J. Shah, A. Zada, Chitosan-coated cotton cloth supported copper nanoparticles for toxic dye reduction, Int. J. Biol. Macromol. 111 (2018) 832-838.

[23] N. N. Krishnan, S. Lee, R. V. Ghorpade, A. Konovalova, J. H. Jang, H. Kim, J. Han, D. Henkensmeier, H. Han, Polybenzimidazole (PBI-OO) based composite membranes using sulfophenylated TiO_2 as both filler and crosslinker, and their use in the HT-PEM fuel cell, J. Membr. Sci. 560 (2018) 11-20; doi.org/10.1016/j.memsci.2018.05.006

[24] C. Jin, X. Zhu, S. Zhang, S. Li, Highly conductive flexible alkylsulfonated side chains poly(phthalazinone ether ketone) for proton exchange membranes, Polymer 148 (2018) 269-277. doi.org/10.1016/j.polymer.2018.06.04

[25] L.J. Bonderer, A.R. Studart, L.J. Gauckler, Bioinspired design and assembly of platelet reinforced polymer films, Science 319 (2008) 1069, doi:10.1126/science.1148726

[26] R. Khan, M. Dhayal, Chitosan/polyaniline hybrid conducting biopolymer base impedimetric immunosensor to detect ochratoxin-A, Biosens. Bioelectron. 24 (2009) 1700-1705. doi.org/10.1016/j.bios.2008.08.046

[27] Q. Y. Huai, Y. M. Zuo, Synthesis of porous titaniaspheres for HPLC by polymerization-induced colloid aggregation (PICA) using tert-n-butyl titanate, J. Anal. Chem. 64 (2009) 176-180. https://doi.org/10.1134/S1061934809020142

[28] S. Ahmed, Y. Cai, M. Ali, S. Khannal, Z. Ahmad, Y. Lu, S. Wang, S. Xu, One-step phosphorylation of graphene oxide for the fabrication of nanocomposite membranes with enhanced proton conductivity for fuel cell applications, J. Mater. Sci.: Mater. Electron. 1 30 (2019) 13056-13066

[29] J. Randon, J. Guerrin, J. Rocca, Synthesis of titania monoliths for chromatographic separations, J. Chromatogr. A 1214 (2008) 183-186. doi.org/10.1016/j.chroma.2008.10.108

[30] S. Mallakpour, A. N. Ezhieh (2018) Citric acid and vitamin c as coupling agents for the surface coating of zro2 nanoparticles and their behavior on the optical, mechanical, and thermal properties of poly(vinyl alcohol) nanocomposite films. J Polym Environ 26: 2813.

[31] Q. Shi, Q. Li, D. Shan, Q. Fan, H. Xue, Biopolymer-clay nanoparticles composite system (chitosan-laponite) for electrochemical sensing based on glucose oxidase, Mater. Sci. Eng. C 28 (2008) 1372-1375, doi.org/10.1016/j.msec.2008.03.001

[32] A. R. A. Rahman, G. Justin, A. G. Elie, Towards an implantable biochip for glucose and lactate monitoring using microdisc electrode arrays (MDEAs), Biomedical Microdevices (2008) doi.org/10.1007/s10544-008-9211-6

[33] V. B. Kandimalla, V. S. Tripathi, H. Ju, Immobilization of biomolecules in sol-gels: Biological and analytical applications, Critical Rev. Anal. Chem. 36 (2006) 73-106. doi.org/10.1080/10408340600713652

[34] M. Rabipour, Z. S. Pour, R. Sahraei, M. Ghaemy, M. E. Jazi, T. E. Mlsna (2020) pH-sensitive nanocomposite hydrogels based on poly(vinyl alcohol) macromonomer and graphene oxide for removal of cationic dyes from aqueous solutions. J Polym Environ 28:584.

[35] L. Ma, H. Luo, J. Dai, P. W. Carr, Development of acid stable, hyper-crosslinked, silica-based reversed-phase liquid chromatography supports for the separation of organic bases, J. Chromatogr. A 1114 (2006) 21-28, doi.org/10.1016/j.chroma.2006.02.017

[36] T. Kim, K. Alhooshani, A. Kabir, D. Fries, A. Malik, High pH-resistant, surface-bonded sol-gel titania hybrid organic–inorganic coating for effective on-line hyphenation of capillary microextraction (in-tube solid-phase microextraction) with high-performance liquid chromatography, J. Chromatogr. A 1047 (2004) 165-174, doi.org/10.1016/S0021-9673(04)01027-1

[37] T. Zhang, B. Tian, J. Kong, P. Yang, B. Liu, A sensitive mediator-free tyrosinase biosensor based on an inorganic-organic hybrid titania sol-gel matrix, Anal. Chim. Acta 489 (2003) 199-206, doi.org/10.1016/S0003-2670(03)00758-X

[38] J. Yu, H. Ju, Amperometric biosensor for hydrogen peroxide based on hemoglobin entrapped in titania sol-gel film, Anal. Chim. Acta 486 (2003) 209-216, doi.org/10.1016/S0003-2670(03)00508-7

[39] L. S. Grundy, V. E. Lee, N. Li, C. Sosa, W. D. Mulhearn, R. Liu, R. A. Register, A. Nikoubashman, R. K. Prud'homme, A. Z. Panagiotopoulos, R. D. Priestley, Rapid production of internally structured colloids by flash nanoprecipitation of block copolymer blends, ACS Nano 12 (2018) 4660-4668, doi.org/10.1021/acsnano.8b01260

[40] M. A. Otache, R. U. Duru, O. Achugasim, O. J. Abayeh (2021) Advances in the modification of starch via esterification for enhanced properties. J Polym Environ. https://doi.org/10.1007/s10924-020-02006-0.

[41] Z. Kahlerras, R. Irinislimane, S. Bruzaud, N. B. Bensemra (2020) Elaboration and characterization of polyurethane foams based on renewably sourced polyols. J Polym Environ 28:3003.

[42] A. Zada, P. Muhammad, W. Ahmad, Z. Hussain, S. Ali, M. Khan, Q. Khan, M. Maqbool, Surface plasmonic-assisted photocatalysis and optoelectronic devices with noble metal nanocrystals: design, synthesis, and applications, Adv. Funct. Mater. 30 (7) (2020) 1906744.

[43] X. Chu, Y. Qu, A. Zada, L. Bai, Z. Li, F. Yang, L. Zhao, G. Zhang, X. Sun, Z. Yang, L. Jing, Ultrathin phosphate-modulated Co phthalocyanine/g-C3N4 heterojunction photocatalysts with single Co-N_4 sites for efficient O_2 activation, Adv. Sci. 7 (16) (2020) 2001543.

[44] A. Zada, Y. Qu, S. Ali, N. Sun, H. Lu, R. Yan, X. Zhang, L. Jing, Improved visible-light activities for degrading pollutants on TiO_2/g-C_3N_4 nanocomposites by decorating SPR Au nanoparticles and 2,4-dichlorophenol decomposition path, J. Hazard. Mater. 342 (2018) 715-723.

[45] W. Ali, H. Ullah, Amir Zada, W. Muhammad, S. Ali, S. Shaheen, M. K. Alamgir, M. Z. Ansar, Z. Ullah Khan, H. Bilal, P. S. Yap, Synthesis of TiO_2 modified self-assembled honeycomb ZnO/SnO_2 nanocomposites for exceptional photocatalytic degradation of 2,4-dichlorophenol and bisphenol A, Sci. Total Environ. 746 (2020) 141291.

[46] C. Liu, F. Raziq, Z. Li, Y. Qu, A. Zada, L. Jing, Synthesis of TiO_2/g-C_3N_4 nanocomposites with phosphate-oxygen functional bridges for improved photocatalytic activity, Chin. J. Catal. 38(6) (2017) 1072-1078.

[47] K. Qi, S. Liu, A. Zada, Graphitic carbon nitride, a polymer photocatalyst, J. Taiwan Inst. Chem. Eng. 109 (2020) 111-123.

[48] A. Zada, N. Ali, F. Subhan, N. Anwar, M. I. A. Shah, M. Ateeq, Z. Hussain, K. Zaman, M. Khan, Suitable energy platform significantly improves charge separation of g-C3N4 for CO2 reduction and pollutant oxidation under visible-light, Prog. Nat. Sci. Mat. Int. 29 (2019) 138-144.

[49] M. Xu, A. Zada, R. Yan, H. Li, N. Sun, Y. Qu, Ti_2O_3/TiO_2 heterophase junctions with enhanced charge separation and spatially separated active sites for photocatalytic CO_2 reduction, Phys. Chem. Chem. Phys. 22 (2020) 4526-4532.

[50] A. Zada, M. Khan, M. A. Khan, Q. Khan, A. H. Yangjeh, A. Dang, M. Maqbool, Review on the hazardous applications and photodegradation mechanisms of chlorophenols over different photocatalysts, Environ. Res. 195 (2021) 110742.

[51] S. T. Koev, P. H. Dykstra, X. Luo, G. W. Rubloff, W. E. Bentley, G. F. Payne, R. Ghodssi. Chitosan: an integrative biomaterial for lab-on-a-chip devices, Lab on a Chip 10 (2010) 3026, doi.org/10.1039/c0lc00047

[52] L. Yang, X. Lin, X. Zhang, W. Zhang, A. Cao, L. Wan, General synthetic strategy for hollow hybrid microspheres through a progressive inward crystallization process, J. Am. Chem. Soc. 138 (2016) 5916-5922, doi.org/10.1021/jacs.6b00773

[53] M. Wang, Z. Sun, Q. Yue, J. Yang, X. Wang, Y. Deng, C. Yu, D. Zhao, An interface-directed coassembly approach to synthesize uniform large-pore mesoporous silica spheres, J. Am. Chem. Soc. 136 (2014) 1884-1892, doi.org/10.1021/ja4099356

[54] K. Du, D. Yang, Y. Sun, Controlled fabrication of porous titania beads by a sol-gel templating method, Ind. Eng. Chem. Res. 48 (2009) 755-762, doi.org/10.1021/ie8011165

[55] T. E. Thingholm, M. R. Larsen, C. R. Ingrell, M. Kassem, O. N. Jensen, TiO_2-based phosphoproteomic analysis of the plasma membrane and the effects of phosphatase inhibitor treatment, J. Proteome Res. 7 (2008) 3304-3313, doi.org/10.1021/pr800099y

[56] Y. Xu, D. Chen, X. Jiao, K. Xue, Nanosized Cu_2O/PEG400 composite hollow spheres with mesoporous shells, J. Phys. Chem. C 111 (2007) 16284-16289, doi.org/10.1021/jp075358x

[57] M. Khan, A. Hamid, L. Tiehu, A. Zada, F. Attique, N. Ahmad, A. Ullah, A. Hayat, I. Mahmood, A. Hussain, Y. Khan, I. Ahmad, A. Ali, T. K. Zhao, Surface optimization of detonation nanodiamonds for the enhanced mechanical properties of polymer/nanodiamond composites, Diamond Relat. Mater. 107 (2020) 107897.

[58] M. W. H. Pinkse, P. M. Uitto, M. J. Hilhorst, B. Ooms, A.t J. R. Heck, Selective isolation at the femtomole level of phosphopeptides from proteolytic digests using 2D-NanoLC-ESI-MS/MS and titanium oxide Precolumns, Ana. Chem. 76 (2004) 3935-3943, doi.org/10.1021/ac0498617

[59] J. Yu, H. Ju, Preparation of porous titania sol-gel matrix for immobilization of horseradish peroxidase by a vapor deposition method, Ana. Chem. 74 (2002) 3579-3583, doi.org/10.1021/ac011290k

Figures

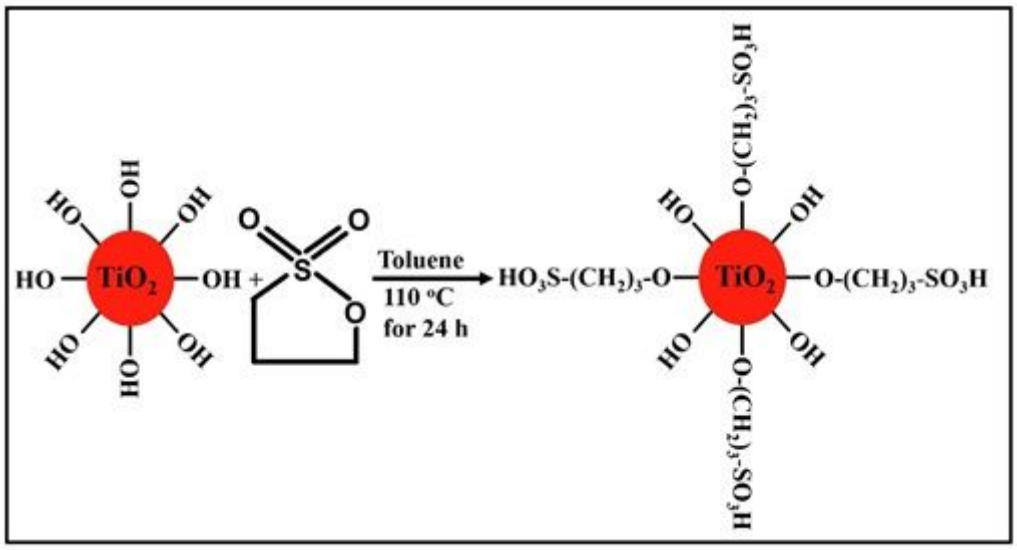

Figure 1

Schematic for the sulfonation of nano-TiO2.

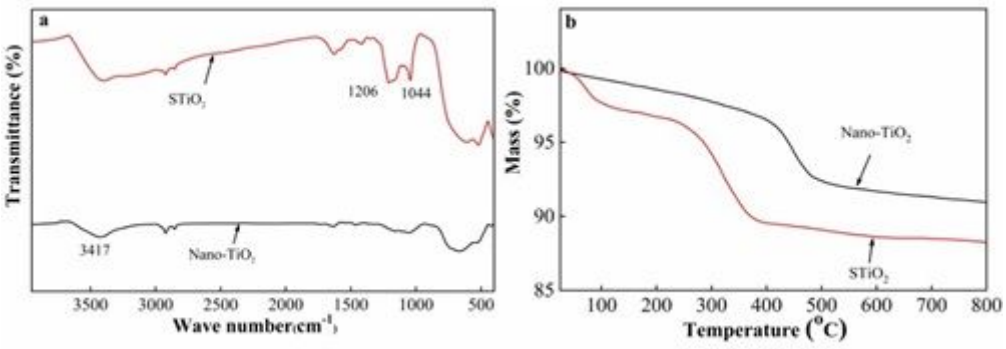

Figure 2

FTIR (a) and TGA analysis of TiO2 and STiO2 particles (b).

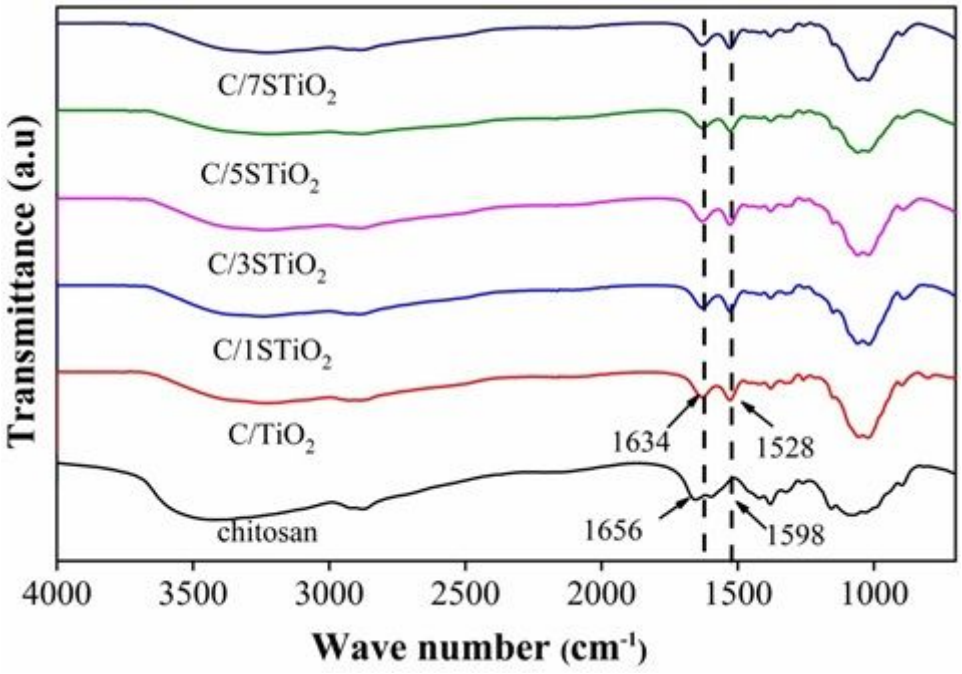

Figure 3

The FTIR spectra of chitosan and C/STiO2 nanocomposite membranes.

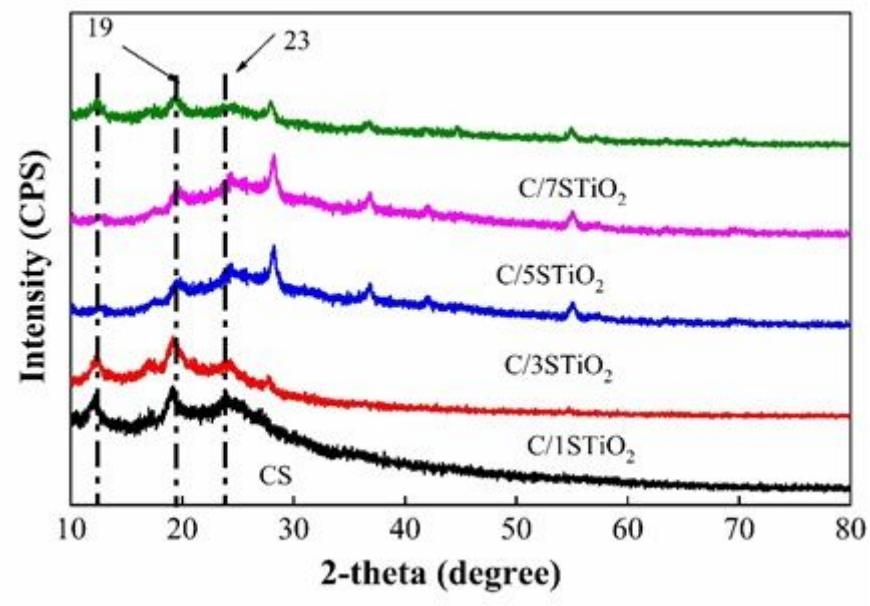

Figure 4

The XRD patterns of chitosan control and C/STiO2 nanocomposite membranes.

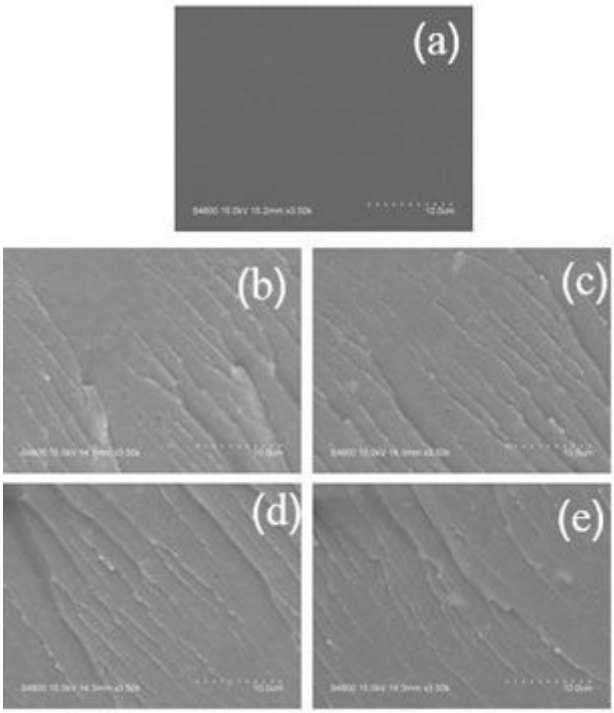

Figure 5

SEM images of cryo-fractured surfaces of chitosan control and C/STiO2 nanocomposite membranes with different STiO2 contents, chitosan (a), C/1STiO2 (b), C/3STiO2 (c), C/5STiO2 (d), and C/7STiO2 (e).

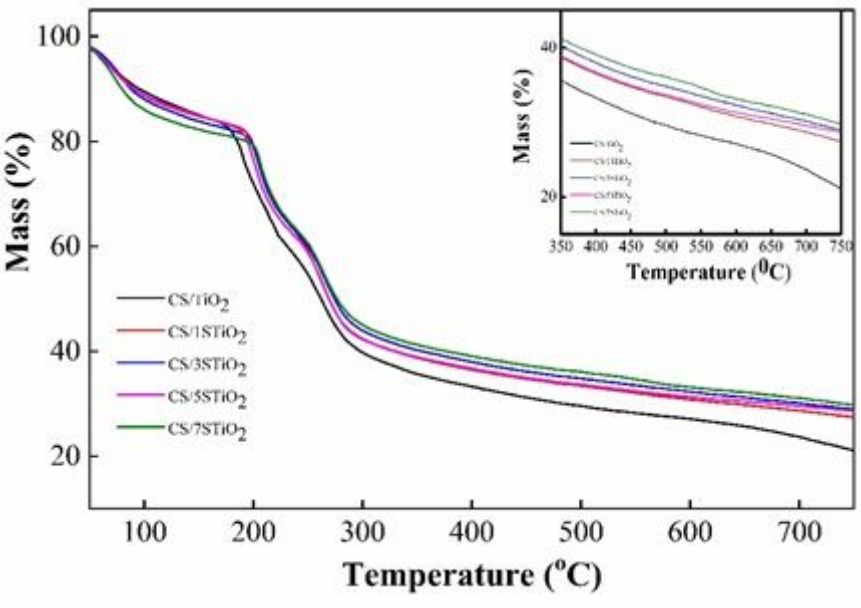

Figure 6

TGA curves of chitosan control and C/STiO2 nanocomposite membranes

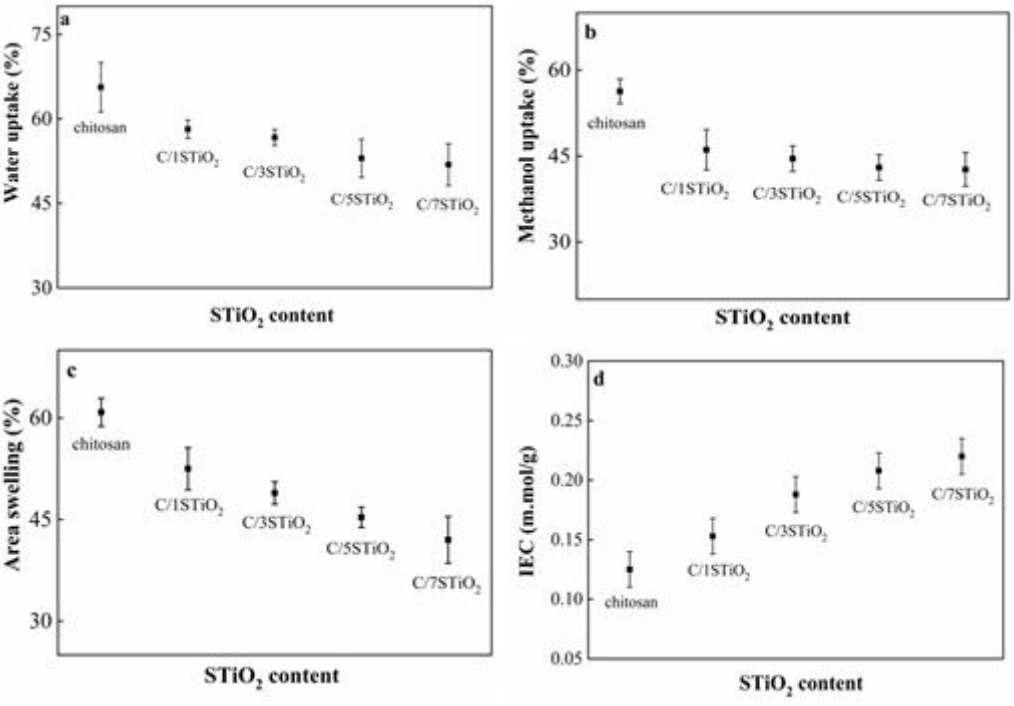

Figure 7

Water uptake(a), methanol uptake(b), area swelling (c) and IEC (d) of chitosan and C/STiO2 membranes at room temperature.

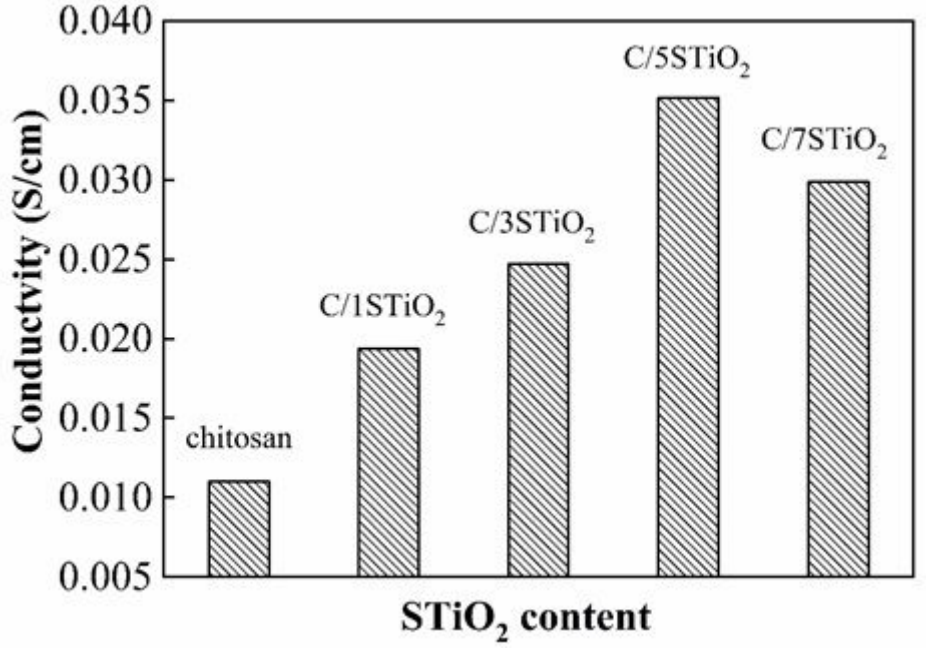

Figure 8

Proton conductivity of chitosan control and C/STiO2 nanocomposite membranes